Anal Bioanal Chem (2004) 379: 920–930
DOI 10.1007/s00216-004-2708-9

REVIEW

Amanda J. Haes · Richard P. Van Duyne

A unified view of propagating and localized surface plasmon resonance biosensors

Received: 30 March 2004 / Revised: 2 June 2004 / Accepted: 3 June 2004 / Published online: 28 July 2004

Abstract The intense colors of noble metal nanoparticles have inspired artists and fascinated scientists for hundreds of years. In this review, we describe refractive index sensing platforms based on the tunability of the localized surface plasmon resonance (LSPR) of arrays of silver nanoparticles and of single nanoparticles. Specifically, the color associated with single nanoparticles and surface-confined nanoparticle arrays will be shown to be tunable and useful as platforms for chemical and biological sensing. Finally, the LSPR nanosensor will be compared to traditional, flat surface, propagating surface plasmon resonance sensors.

Keywords Localized surface plasmon resonance · Nanosensor · Single nanoparticle · Spectroscopy · Biosensing

Introduction

The intense scattering and absorption of light from noble metal nanoparticles is the source of the beautiful colors in stained glass windows and has attracted the interest of scientists for generations. Although scientists have learned that the characteristic hues of these noble metal nanoparticle suspensions arise from their strong interaction with light, the advent of the field of nanoparticle optics has allowed a deep understanding of the relationship between material properties such as composition, size, shape, and local dielectric environment and the observed color of a metal suspension. An understanding of the optical properties of noble metal nanoparticles holds both fundamental and practical significance. Fundamentally, it is important to systematically explore the nanoscale structural and local environmental characteristics that cause optical property variation as well as providing access to regimes of predictable behavior. Practically, the tunable optical properties of nanostructures can be applied as materials for surface-enhanced spectroscopy [1–5], optical filters [6, 7], plasmonic devices [8–11], and sensors [12–26].

Noble metal nanoparticles exhibit a strong UV-visible (UV-vis) absorption band that is not present in the spectrum of the bulk metal [27–34]. This absorption band results when the incident photon frequency is resonant with the collective oscillation of the conduction electrons and is known as the localized surface plasmon resonance (LSPR). LSPR excitation results in wavelength-selective absorption with extremely large molar extinction coefficients of approximately 3×10^{11} M^{-1} cm^{-1} [35], resonant Rayleigh scattering [36, 37] with an efficiency equivalent to that of 10^6 fluorophors [38], and the enhanced local electromagnetic fields near the surface of the nanoparticle, which are responsible for the intense signals observed in all surface-enhanced spectroscopies [3, 18, 19].

The simplest theoretical approach available for modeling the optical properties of nanoparticles is the Mie theory estimation of the extinction of a metallic sphere in the long-wavelength, electrostatic dipole limit. In the following equation [39]:

$$E(\lambda) = \frac{24\pi N_A a^3 \varepsilon_m^{3/2}}{\lambda \ln(10)} \left[\frac{\varepsilon_i}{(\varepsilon_r + \chi\varepsilon_m)^2 + \varepsilon_i^2} \right] \quad (1)$$

$E(\lambda)$ is the extinction (viz., sum of absorption and scattering), N_A is the areal density of nanoparticles, a is the radius of the metallic nanosphere, ϵ_m is the dielectric constant of the medium surrounding the metallic nanosphere (assumed to be a positive, real number and wavelength independent), λ is the wavelength of the absorbing radiation, ϵ_i is the imaginary portion of the metallic nanoparticle's dielectric function, ϵ_r is the real portion of the metallic nanoparticle's dielectric function, and χ is the term that describes the aspect ratio of the

A. J. Haes · R. P. Van Duyne (✉)
Department of Chemistry, Northwestern University,
2145 Sheridan Road, Evanston,
IL, 60208-3113, USA
E-mail: vanduyne@chem.northwestern.edu

nanoparticle (equal to two for a sphere). It is abundantly clear that the LSPR spectrum of an isolated metallic nanosphere embedded in an external dielectric medium will depend on the nanoparticle radius a, the nanoparticle material (ϵ_i and ϵ_r), and the nanoenvironment's dielectric constant (ϵ_m). Furthermore, when the nanoparticles are not spherical, as is always the case in real samples, the extinction spectrum will depend on the nanoparticle's in-plane diameter, out-of-plane height, and shape (χ). The values for χ increase from two (for a sphere) up to, and beyond, values of 17 for a 5:1 aspect ratio nanoparticle. In addition, many of the samples considered in this work contain an ensemble of nanoparticles that are supported on a substrate. Thus, the LSPR will also depend on interparticle spacing and substrate dielectric constant.

It is apparent from Eq. 1 that the location of the extinction maximum of noble metal nanoparticles is highly dependent on the dielectric properties of the surrounding environment, and that wavelength shifts in the extinction maximum of nanoparticles can be used to detect molecule-induced changes surrounding the nanoparticle. As a result, there are at least four different nanoparticle-based sensing mechanisms that enable the transduction of macromolecular or chemical-binding events into optical signals based on changes in the LSPR extinction or scattering intensity shifts in LSPR λ_{max}, or both. These mechanisms are: (1) resonant Rayleigh scattering from nanoparticle labels in a manner analogous to fluorescent dye labels [37, 38, 40–46], (2) nanoparticle aggregation [47–52], (3) charge-transfer interactions at nanoparticle surfaces [39, 53–57], and (4) local refractive index changes [12, 15–17, 19, 20, 53, 58–62].

In order to systematically study the LSPR response of noble metal nanoparticles to changes in their dielectric environment, a technique that produces nanoparticles with size and shape monodispersity is required. The chemical synthesis of noble metal nanostructures is often employed for this purpose [63–70]. These approaches are used to prepare high concentrations of a variety of shapes and sizes of nanoparticles with varying degrees of monodispersity and tunable optical properties (Fig. 1). For solution-phase LSPR-based sensing, signal transduction depends on the sensitivity of the surface plasmon to interparticle coupling. When there are multiple particles in solution that support a localized surface plasmon and are in close proximity (i.e., interparticle spacings less than the nanoparticle diameter), they are able to interact electromagnetically through a dipole coupling mechanism. This broadens and red shifts the LSPR, a change easily monitored by using UV-vis spectroscopy. Two methods of detection readily lend themselves to monitoring these changes in the position of the LSPR UV-vis extinction (absorption plus scattering) and resonant Rayleigh scattering spectroscopy.

Several papers have been published on a gold nanoparticle based UV-vis technique for the detection of DNA. This colorimetric detection method is based on the change in absorbance spectra (i.e., color) as particles are brought together by the hybridization of complementary DNA strands [13, 41, 48, 50–52, 71]. The limits of detection (LOD) reported are in the range of tens of femtomoles of target oligonucleotide. These nanoparticle aggregation assays represent a 100-fold increase in sensitivity over conventional fluorescence-based assays [41].

Recently, gold nanoshells, that is, silica beads with a thin gold coating, have been used to detect antigens in whole blood [14]. In these studies, gold nanoshells were functionalized with a specific immunoglobulin. The nanoshells were designed such that they exhibit plasmon resonances in the near-infrared between the water absorption band and the absorption of hemoglobin. Upon addition of the nanoshells to whole blood that contains the appropriate antigen, the plasmon resonance broadens, the intensity decreases, and a slight red shift in the plasmon resonance occurs. This immunoassay, which occurs in less than 30 min, is capable of detecting picogram/milliliter quantities of antigens.

An alternative approach to solution-phase nanoparticle sensing is to attach chemically synthesized nanoparticles to substrates. By using this method, gold nanoparticles can be chemically attached in a random fashion to a transparent substrate to detect proteins [24, 58]. In this format, signal transduction depends on changes in the nanoparticles' dielectric environment induced by solvent or target molecules (not via nanoparticle coupling). By using this chip-based approach, a solvent refractive index sensitivity of 76.4 nm RIU^{-1} has been found and a detection of 16 nM streptavidin can be achieved [24, 58]. This approach has many advantages including: (1) a simple fabrication technique that can be performed in most labs, (2) real-time biomolecule detection using UV-vis spectroscopy, and (3) a chip-based design that allows for multiplexed analysis.

A similar approach for biomolecule detection can be implemented by using homogeneous, regularly spaced nanoparticles that are adhered to a substrate. To make these nanoparticles, nanosphere lithography (NSL) [72], a powerful fabrication technique that inexpensively produces arrays of nanoparticles with controlled shape, size, and interparticle spacing, can be employed. NSL begins with the self-assembly of size-monodisperse nanospheres of diameter (D), to form a 2D colloidal crystal deposition mask. A substrate is prepared so that the nanospheres freely diffuse until they reach their lowest energy configuration. This is achieved by chemically modifying the nanosphere surface with a negative charge that is electrostatically repelled by the negatively charged substrate such as mica or chemically treated glass. As the solvent (water) evaporates, capillary forces draw the nanospheres together, and they crystallize in an hexagonally close-packed pattern on the substrate. As in all naturally occurring crystals, nanosphere masks include a variety of defects that arise as a result of nanosphere polydispersity, site randomness, point defects (vacancies), line defects (slip dislocations), and

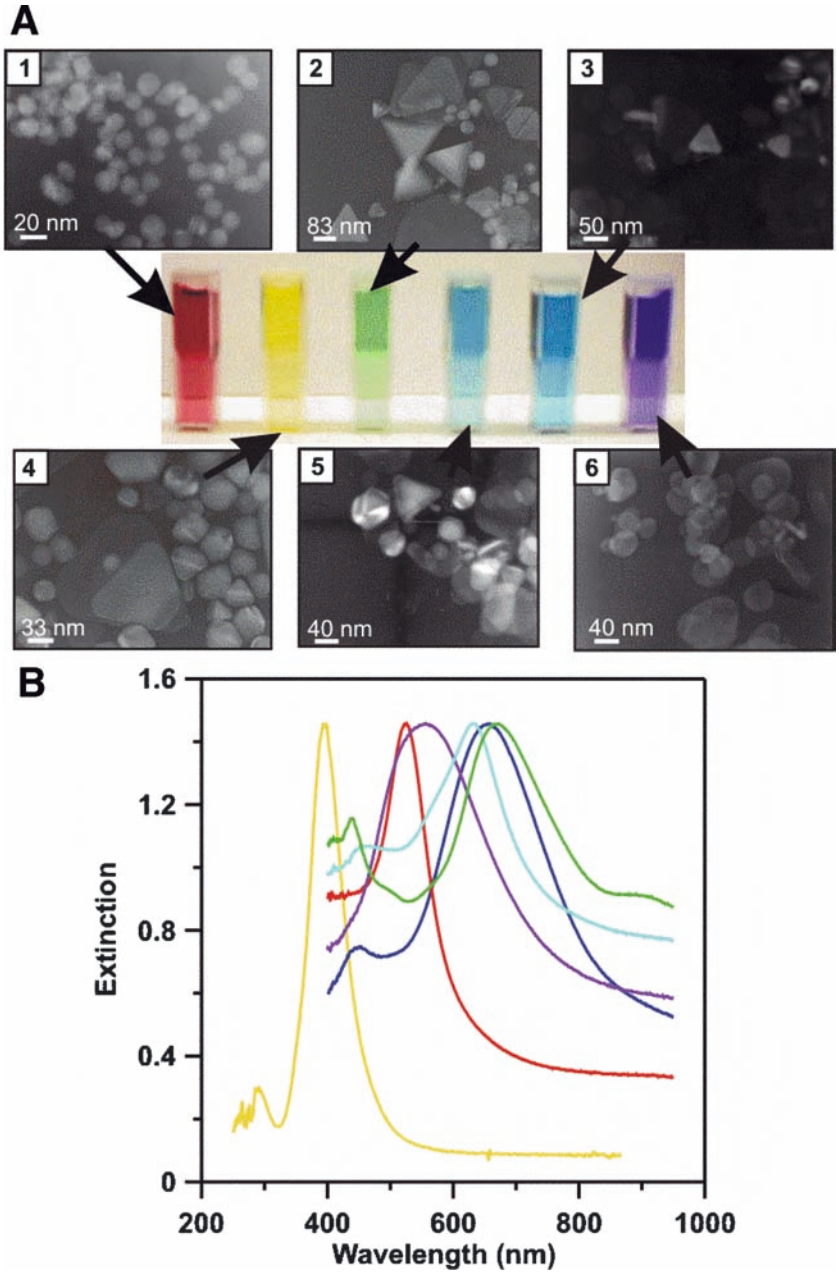

Fig. 1a, b Tunable Ag and Au nanoparticle solutions. **a** Corresponding transmission electron micrographs. *1* The red solution consists of homogeneous Au nanospheres (13-nm diameter). *4* The yellow solution consists of inhomogeneous Ag nanoparticles (nanospheres, trigonal prisms, and polygon platelets). *2* The green solution consists of Ag nanoparticles (nanospheres, trigonal prisms, and polygon platelets). *5* The light blue solution consists of Ag nanoparticles (trigonal prisms and polygon platelets). *3* The dark blue solution consists of Ag nanoparticles (trigonal prisms with rounded tips and polygon platelets). *6* The purple solution is made up of inhomogeneous oblong Ag nanoparticles. **b** UV-vis extinction spectra of the corresponding solutions (*color of line* corresponds to solution color)

polycrystalline domains. Typical defect-free domain sizes are in the 10- to 100-μm range. Following self-assembly of the nanosphere mask, a metal or another material is then deposited by thermal evaporation, electron beam deposition, or pulsed laser deposition from a collimated source normal to the substrate through the nanosphere mask to a controlled mass thickness, d_m. After metal deposition, the nanosphere mask is removed, typically by sonicating the entire sample in a solvent, leaving behind surface-confined nanoparticles that have a triangular footprint. The optical properties of these nanoparticles can be easily tuned throughout the visible region of the spectrum by changing the size or shape of the nanoparticles (Fig. 2).

Experimental details for LSPR sensing on nanoparticle arrays

By using NSL, we have demonstrated that nanoscale chemosensing and biosensing can be realized through shifts in the LSPR extinction maximum (λ_{max}) of these triangular silver nanoparticles [12, 15, 20, 53]. Instead of being caused by electromagnetic coupling between the nanoparticles, these wavelength shifts are caused by adsorbate-induced local refractive index changes in competition with charge-transfer interactions at the surfaces of nanoparticles. It should be noted that the signal transduction mechanism in this nanosensor is a

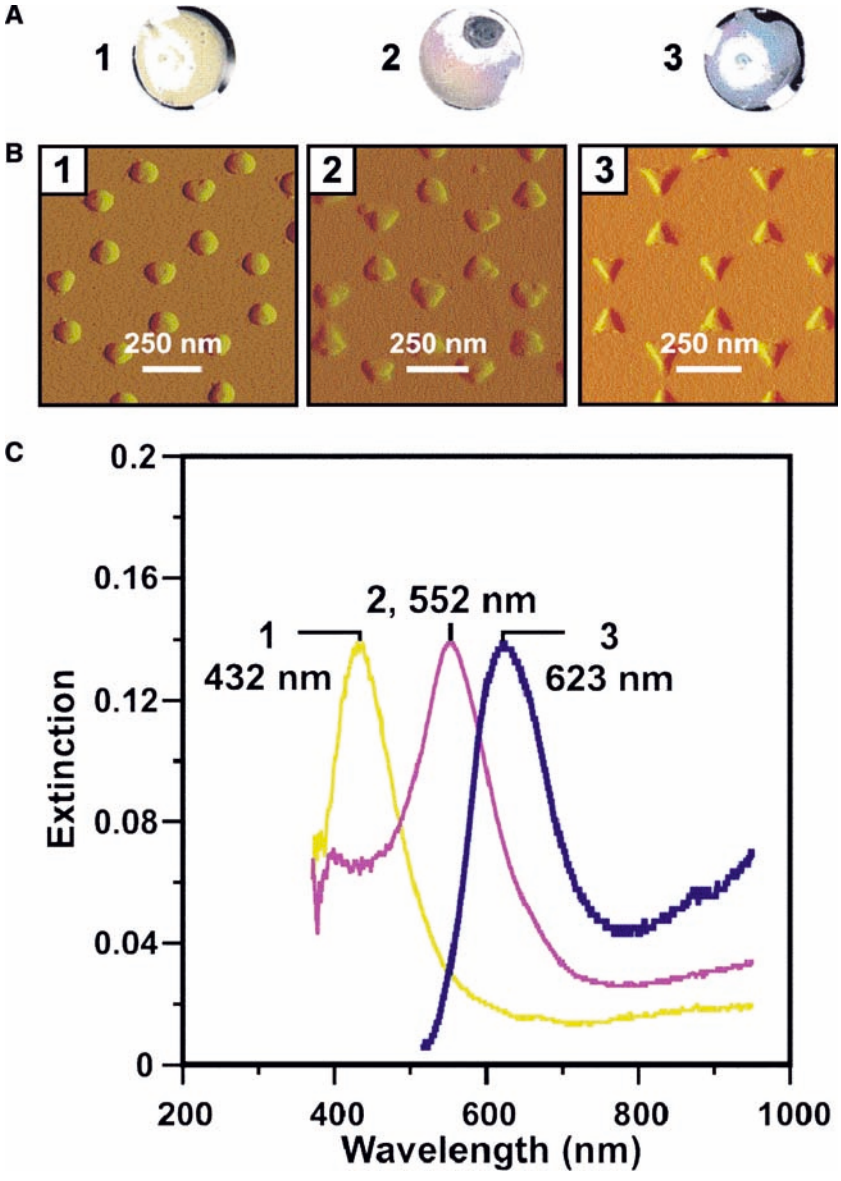

Fig. 2 Tunable Ag nanoparticle substrates fabricated by using NSL. *Top* Photographs of nanoparticle substrates. *Middle* AFM images of nanoparticle substrates. *Bottom* UV-vis extinction spectra of Ag nanoparticle substrates. Ag nanoparticle substrate ($D = 400$ nm, $d_m = 50.0$ nm) *1* after thermal in vacuum for 1 h at 600°C, *2* after thermal annealing in vacuum for 1 h at 300°C, and *3* as fabricated (no annealing)

reliably measured wavelength shift rather than an intensity change as in many previously reported nanoparticle-based sensors.

For these experiments, macroscale UV-vis extinction spectra were collected in standard transmission geometry with unpolarized light using an Ocean Optics spectrophotometer (SD2000). The peak-to-peak wavelength shift noise of the baseline in repetitive experiments from this spectrophotometer is approximately 0.5 nm. By taking the LOD as three times this value, one can conservatively estimate that the LOD of an assay will arise from a wavelength shift of 1.5 nm. The probe beam diameter was approximately 2 mm. A home-built flow cell was used to control the external environment of the Ag nanoparticle substrates (Fig. 3). It should be noted that this entire system (minus the nanoparticle substrate) costs about US $4,500. 11-Mercaptoundecanoic acid (11-MUA; 95% purity), 1-octanethiol (1-OT; 98.5% purity), hexadecanethiol (92% purity), hexanes, and methanol were purchased from Aldrich (Milwaukee, WI, USA). Anti-biotin, 1-ethyl-3-[3-dimethylaminopropyl]carbodiimide (EDC) hydrochloride, streptavidin, 10 mM and 20 mM phosphate-buffered saline (PBS) pH 7.4 was obtained from Sigma (St. Louis, MO, USA). (+)-Biotinyl-3,6-dioxaoctanediamine (biotin) was purchased from Pierce (Rockford, IL, USA). Absolute ethanol was purchased from Pharmco (Brookfield, CT, USA). Ag wire (99.95%, 0.5 mm) was purchased from D.F. Goldsmith (Evanston, IL, USA). Borosilicate glass substrates were purchased from Fisher Scientific (Pittsburgh, PA, USA). Polystyrene nanospheres with diameters of 400 ± 7 nm (Interfacial Dynamics, Portland, OR, USA) were received as a suspension in water. All materials used in these experiments were used as received.

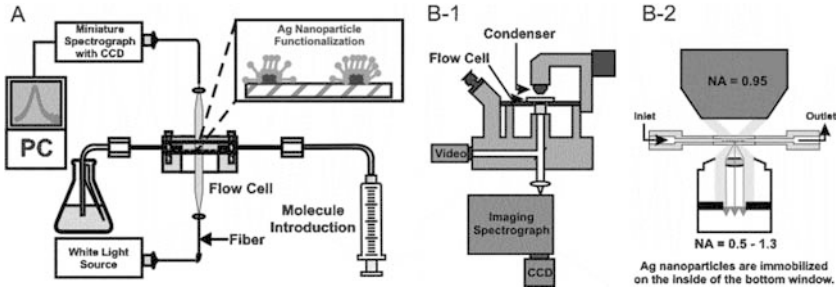

Fig. 3 *Left* Instrumental diagram for the array-based LSPR nanosensor experiments. The flow cell is fiber optically coupled to a white light source and miniature spectrometer. The cell is linked directly to either a solvent reservoir or to a syringe containing the desired analyte. *Middle* Instrumental diagram used for single nanoparticle spectroscopy. *Right* Close-up of the flow cell to show illumination and collection geometry

Chemosensing using LSPR spectroscopy on Ag nanoparticle arrays

The Ag nanotriangles have in-plane widths of approximately 100 nm and out-of-plane heights of about 51 nm as determined by atomic force microscopy (AFM) (Fig. 4). For this study, the samples were incubated in 1.0 mM concentrations of hexadecanethiol ethanolic solution for 18–24 h. The difference between the extinction maximum before and after incubation is the wavelength shift response reported. Figure 4 shows the UV-vis extinction spectra of Ag nanoparticles (perpendicular bisector (a) = 100 nm, height (b) = 50.0 nm) in an N_2 environment before and after chemical modification with hexadecanethiol. Monolayer modification causes the λ_{max} to shift to the red from 595 to 635 nm.

Fig. 4 A depiction of the LSPR nanobiosensor is shown. *Left* Tapping-mode AFM image of the Ag nanoparticles (D = 390 nm; d_m = 50.0 nm Ag on a mica substrate, scan area, 3.0 μm^2) was collected. After solvent annealing, the resulting nanoparticles have in-plane widths of approximately 100 nm and out-of-plane heights of about 51 nm. *Right* LSPR spectra of nanoparticles (width = 100 nm, height = 50.0 nm) in a nitrogen environment. *1* Ag nanoparticles before chemical modification, λ_{max} = 594.8 nm and *2* after modification with 1 mM hexadecanethiol, λ_{max} = 634.8 nm

Given the surface area of a single nanoparticle (1.4×10^{-10} cm^2 nanoparticle^{-1}) and the packing density (4.4×10^{14} molecules cm^{-2}) of hexadecanethiol on silver, one can estimate that this shift arises from approximately 60,000 molecules per nanoparticle. While this number does not reflect the overall solution concentration, it does indicate that if a single nanoparticle was exposed to only 60,000 molecules, a maximum wavelength shift response could be obtained.

Demonstration of LSPR sensing on single nanoparticles

In the previous experiment, the sensor response was attributed to the assembly of 60,000 hexadecanethiol molecules per nanoparticle on approximately 10^{10} nanoparticles. An obvious method to improve the LOD (in terms of molecules detected) of the system would be to reduce the number of nanoparticles probed. A key to exploiting single nanoparticles as sensing platforms is to develop a technique to monitor the LSPR of individual nanoparticles with a reasonable signal-to-noise ratio. UV-vis absorption spectroscopy does not provide a practical means of accomplishing this task. Even under the most favorable experimental conditions, the absorbance of a single nanoparticle is very close to the shot noise-governed LOD. Instead, resonant Rayleigh scattering spectroscopy is the most straightforward means of characterizing the optical properties of individual metallic nanoparticles. Similar to fluorescence spectroscopy, the advantage of scattering spectroscopy lies in the fact that the scattering signal is being detected in the presence of a very low background. The instrumental approach for performing these experiments generally

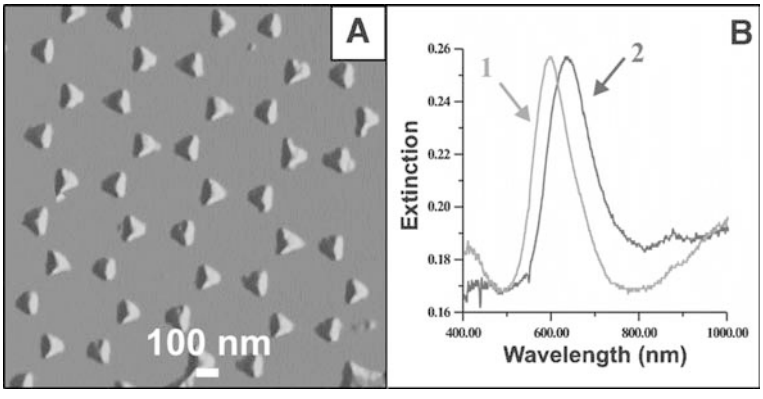

involves using high-magnification microscopy coupled with oblique or evanescent illumination of the nanoparticles. Klar et al. [73] utilized a near-field scanning optical microscope coupled to a tunable laser source to measure the scattering spectra of individual gold nanoparticles embedded in a TiO_2 film. Sonnichsen et al. [42] were able to measure the scattering spectra of individual electron beam lithography-fabricated nanoparticles by using conventional light microscopy. Their technique involved illuminating the nanoparticles with the evanescent field produced by total internal reflection of light in a glass prism. The light scattered by the nanoparticles was collected with a microscope objective and coupled into a spectrometer for analysis. Matsuo and Sasaki [74] employed differential interference contrast microscopy to perform time-resolved laser scattering spectroscopy of single silver nanoparticles. Mock et al. [75] correlated conventional dark-field microscopy and TEM in order to investigate the relationship between the structure of individual metallic nanoparticles and their scattering spectra. These authors have also used the same light microscopy techniques to study the response of the scattering spectrum to the particle's local dielectric environment by immersing the nanoparticle in oils of various refractive indexes [76]. The extension of LSPR sensing to the single nanoparticle limit provides several improvements over existing array- or cluster-based techniques. First, absolute detection limits are dramatically reduced. The surface area of chemically prepared Ag nanoparticles is typically less than 20,000 nm^2, which requires that a complete monolayer of adsorbate must constitute fewer than approximately 100 zeptomole (surface coverage not solution concentration).

Recently, we have demonstrated that by using dark-field microscopy (instrumental diagram, Fig. 3), single Ag nanoparticles can be used to sense local refractive index changes induced via bulk solvent changes and a monolayer of alkanethiols [45]. Just as in the nanoparticle arrays, the use of single nanoparticles as chemosensors was investigated by using alkanethiol adsorbates (Fig. 5). For these experiments, a low density (nanoparticle spacing must be greater than the size of the nanoparticles) of chemically synthesized Ag nanoparticles [63] were dispersed onto a clean glass coverslip. After recording the resonant Rayleigh scattering spectrum of an individual Ag nanoparticle in an N_2 environment [45], a 1.0 mM alkanethiol solution in ethanol was injected into the flow cell. After incubation in the analyte solution, the flow cell was flushed several times with ethanol, methanol, and hexane to ensure that a maximum of one monolayer had adsorbed. Finally, the nanoparticle was dried under N_2 and a scattering spectrum was recorded.

Figure 5 shows a dark-field image of chemically synthesized Ag nanoparticles. The circled nanoparticle was selected and its LSPR λ_{max} response was monitored. Figure 5 displays the scattering spectrum of an individual Ag nanoparticle in nitrogen before ($\lambda_{max} = 510.2$ nm) and after ($\lambda_{max} = 550.9$ nm) modification with a hexadecanethiol monolayer. Based on the average surface area of the nanoparticles prepared and the monolayer packing density of the molecule on Ag, this response corresponds to the detection of fewer than 60,000 surface-confined molecules of hexadecanethiol.

Biosensing on nanoparticle arrays

The large shift induced by a monolayer of small molecules encouraged the pursuit of this line of studies by using biological molecules. The well-studied biotin–streptavidin system with its extremely high binding affinity ($K_a \approx 10^{13}$ M^{-1})[77] was chosen to illustrate the attributes of these LSPR-based nanoscale affinity biosensors. The biotin–streptavidin system has been studied in great detail by surface plasmon resonance (SPR) spectroscopy [78, 79] and serves as an excellent model system for the LSPR nanosensor [12]. Streptavidin, a tetrameric protein, can bind up to four biotinylated molecules (i.e., antibodies, inhibitors, nucleic acids, etc.) with minimal impact on its biological activity [77] and, therefore, will provide a ready pathway for extending

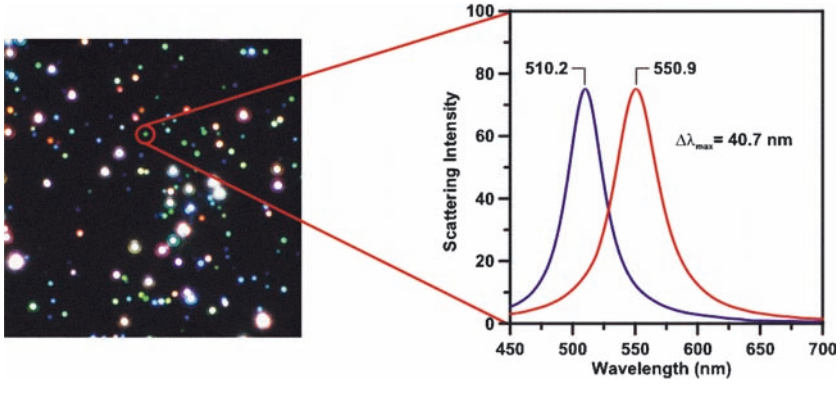

Fig. 5 *Left* A dark-field optical image of a field of Ag nanoparticles. The field of view is approximately 130×170 μm. The nanoparticles were fabricated by citrate reduction of silver ions in aqueous solution and drop-coated onto a glass coverslip. *Right* An individual Ag nanoparticle sensor before and after functionalization with hexadecanethiol. Reproduced with permission from Nano Lett (2003) 3:1057–1062. Copyright 2003 Am Chem Soc

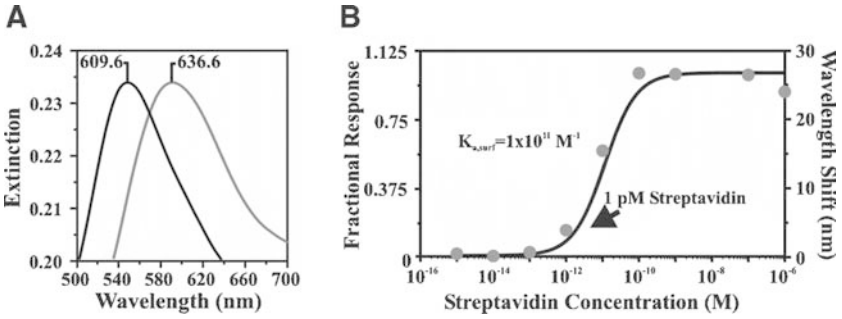

Fig. 6 LSPR spectra illustrating the response of the Ag nanobiosensor to streptavidin corresponding to saturation coverages. All extinction measurements were collected in an N_2 environment. *Left* Ag nanoparticles before ($\lambda_{max} = 609.6$ nm) and after ($\lambda_{max} = 636.6$ nm) 100 nM SA exposure. *Right* The specific binding of streptavidin to the Ag nanobiosensor is shown in the response curve. All measurements were collected in a nitrogen environment. The *solid line* is the calculated value of the nanosensor's response. Reproduced with permission from J Am Chem Soc (2002) 124:10596–10604. Copyright 2002 Am Chem Soc

the analyte accessibility of the LSPR nanobiosensor. In this study, the λ_{max} of the Ag nanoparticles were monitored during each surface functionalization step (Fig. 6). First, the LSPR λ_{max} of the bare Ag nanoparticles was measured to be 561.4 nm (not shown). To ensure a well-ordered monolayer on the Ag nanoparticles, the sample was incubated in the thiol solution for 24 h. After careful rinsing and thorough drying with N_2 gas, the LSPR λ_{max} after modification with the mixed methyl and carboxyl-terminated monolayer (not shown) was measured to be 598.6 nm. The LSPR λ_{max} shift corresponding to this surface functionalization step was a 38-nm red shift with respect to bare Ag nanoparticles; hereafter + will signify a red shift and − a blue shift. Next, biotin was covalently attached via amide bond formation with a two-unit poly(ethylene glycol) linker to carboxylated surface sites. The LSPR λ_{max} after biotin attachment (Fig. 6) was measured to be 609.6 nm, corresponding to an additional +11-nm shift. The LSPR nanosensor has now been prepared for exposure to the target analyte. Exposure to 100 nM streptavidin, resulted in LSPR$\lambda_{max} = 636.6$ nm (Fig. 6), corresponding to an additional +27-nm shift.

The LSPR λ_{max} shift, ΔR, versus [streptavidin] response curve was measured over the concentration range 1×10^{-15} M < [streptavidin] < 1×10^{-6} M (Fig. 6). Each data point is an averaged result from the analysis of three different samples at identical concentrations. The line is not a fit to the data. Instead, the line was computed from a response model. It was found that this response could be interpreted quantitatively in terms of a model involving: (1) 1:1 binding of a ligand to a multivalent receptor with different sites but invariant affinities, and (2) the assumption that only adsorbate-induced local refractive index changes were responsible for the operation of the LSPR nanosensor.

The binding curve provides three important characteristics regarding the system being studied. First, the mass and dimensions of the molecules affect the magnitude of the LSPR shift response. Comparison of the data with theoretical expectations yielded a saturation response, $\Delta R_{max} = 26.5$ nm for streptavidin, a 60-kDa molecule. Next, the surface-confined thermodynamic binding constant $K_{a,surf}$ can be calculated from the binding curve and is estimated to be 1×10^{11} M^{-1} for streptavidin. These numbers are directly correlated to the third important characteristic of the system, the LOD. The LOD of the system corresponds to the smallest wavelength shift response induced by a given solution concentration. These "real" LODs can be translated into a commonly reported surface coverage in terms of molecules. For the NSL-fabricated sensor, the LOD is less than 1 pM (solution concentration) for streptavidin.

Streptavidin sensing with single nanoparticles

We have demonstrated the detection of < 100 streptavidin molecules per nanoparticle (in a solution concentration of 1 pM) by using nanoparticle array sensing. Just as in the hexadecanethiol experiments, a natural method to decrease the total number of molecules sensed would be to decrease the number of nanoparticles probed. Clearly, the ultimate limit to this would be to probe a single nanoparticle and actually detect approximately 100 molecules at our LOD. The biology community would like to reduce the amount of biological sample needed for an assay without amplification. For this reason, we have detected streptavidin on single Ag nanoparticles [46]. First, chemically synthesized Ag nanoparticles that have been dispersed on a glass coverslip are placed in a flow cell, and a dark-field image is collected. The slits on the spectrometer are then narrowed to monitor the scattering spectrum of a single nanoparticle. After functionalization, the LSPR of an individual nanoparticle was measured to be 508.0 nm [Fig. 7(1)]. Next, 10 nM streptavidin was injected into the flow cell, and the nanoparticle was allowed to incubate for 2 h. Following this incubation and rinsing, the λ_{max} of the nanoparticle was measured at 520.7 nm [Fig. 7(2)]. This +12.7-nm shift is estimated to arise from the detection of less than 700 streptavidin molecules. It is hypothesized that just as in the array format, as the streptavidin concentration decreases, a smaller

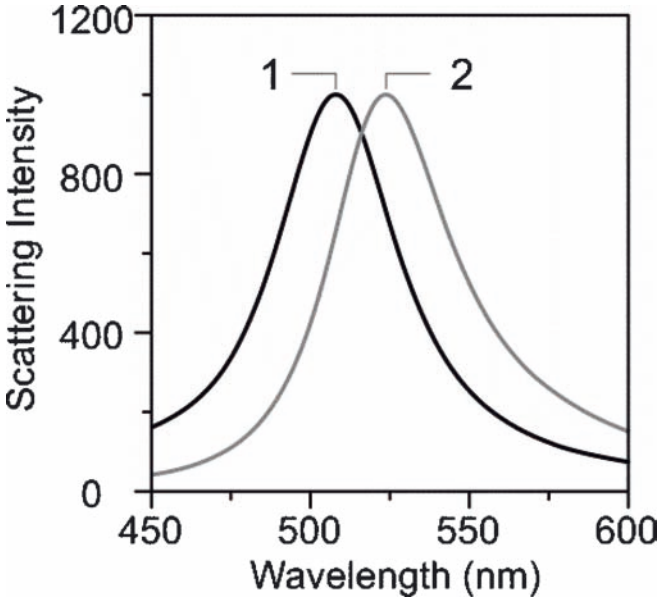

Fig. 7 Individual Ag nanoparticle sensor before and after exposure to 10 nM streptavidin. All measurements were collected in a nitrogen environment. (*1*) Biotinylated Ag nanoparticle, $\lambda_{max} = 508.0$ nm. (*2*) After streptavidin incubation, $\lambda_{max} = 520.7$ nm

number of streptavidin molecules will bind the surface thereby causing smaller wavelength shifts.

Relationship between LSPR and surface plasmon resonance sensors

During the course of these findings, it was realized that the sensor transduction mechanism of this LSPR-based nanosensor is analogous to that of flat surface, propagating SPR sensors (Table 1). For about 20 years, SPR sensors, that is, copper, gold, or silver planar films, have been used as refractive index based sensors to detect analyte binding at or near a metal surface [80] and have been widely used to monitor a broad range of analyte–surface binding interactions including the adsorption of small molecules [78, 81, 82], ligand–receptor binding [79, 83–85], protein adsorption on self-assembled monolayers [86–88], antibody–antigen binding [89], DNA and RNA hybridization [90–93], and protein–DNA interactions [94].

Just as in LSPR spectroscopy, the sensing mechanism of SPR spectroscopy is based on the measurement of small changes in refractive index that occur in response to analyte binding at or near the surface of a noble metal (Au, Ag, Cu) [95]. Chemosensors and biosensors based on SPR spectroscopy possess many desirable characteristics including: (1) a refractive index sensitivity of the order of one part in 10^5–10^6, corresponding to an areal mass sensitivity of approximately 10^{-1} pg mm^{-2} [78, 81, 96]; (2) a long-range sensing length scale determined by the exponential decay of the evanescent electromagnetic field, $L_z \approx 200$ nm [81]; (3) multiple instrumental modes of detection (viz., angle shift, wavelength shift, and imaging) [95]; (4) real-time detection on the 10^{-1}–10^3 s time scale for measurement of binding kinetics [78, 82, 97, 98]; (5) lateral spatial resolution of the order of 10 μm, enabling multiplexing and miniaturization especially using the SPR imaging mode of detection [95]; and (6) the instrument is available commercially.

Important differences to appreciate between the SPR and LSPR sensors are the comparative refractive index sensitivities and the characteristic electromagnetic field decay lengths. SPR sensors exhibit large refractive index sensitivities ($\approx 2\times10^6$ nm RIU^{-1}) [81]. For this reason, the SPR response is often reported as a change in

Table 1 Comparison of SPR and LSPR Sensors

Feature/characteristic	SPR	LSPR
Label-free detection	Yes [79, 82, 91, 99]	Yes [12, 20, 45, 53]
Distance dependence	≈1,000 nm [81]	≈30 nm (size tunable)[18, 19]
Refractive index sensitivity	2×10^6 nm RIU^{-1} [78, 81, 83, 96]	2×10^2 nm RIU^{-1} [18, 53]
Modes	Angle shift [95], wavelength shift, imaging	Extinction [12], scattering [45, 46], imaging [45, 46]
Temperature control	Yes	No
Chemical identification	SPR-Raman	LSPR-SERS
Field portability	No	Yes
Commercially available	Yes	No
Cost	US $150,000–300,000	US $5,000 (multiple particles), US $50,000 (single nanoparticle)
Spatial resolution	≈10×10 μm [95, 100]	1 nanoparticle [45, 46, 76]
Nonspecific binding	Minimal (determined by surface chemistry and rinsing) [95–97, 99, 101]	Minimal (determined by surface chemistry and rinsing) [12]
Real-time detection	Time scale = 10^{-1}–10^3 s, planar diffusion [78, 82, 97, 98, 102]	Time scale = 10^{-1}–10^3 s, radial diffusion [45]
Multiplexed capabilities	Yes [103, 104]	Yes-possible
Small molecule sensitivity	Good [78]	Better [18]
Microfluidics compatibility	Yes	Possible

refractive index units. The LSPR nanosensor, on the other hand, has a modest refractive index sensitivity ($\approx 2\times10^2$ nm RIU^{-1}) [53]. Given that this number is four orders of magnitude smaller for the LSPR nanosensor than the SPR sensor, initial assumptions were made that the LSPR nanosensor would be 10,000 times less sensitive than the SPR sensor. This, however, is not the case. In fact, the two sensors are very competitive in their sensitivities. The short (and tunable) characteristic electromagnetic field decay length, l_d, provides the LSPR nanosensor with its enhanced sensitivity [18, 19]. These LSPR nanosensor results indicate that l_d is approximately 5–15 nm or 1–3% of the light's wavelength and depends on the size, shape, and composition of the nanoparticles. This differs greatly from the 200–300 nm decay length or approximately 15–25% of the light's wavelength for the SPR sensor [81]. The smallest footprint of the SPR and LSPR sensors differs, too. In practice, SPR sensors require at least a 10×10-μm area for sensing experiments. For LSPR sensing, this spot size can be minimized to a large number of individual sensing elements (1×10^{10} nanoparticles for a 2-mm spot size, nanosphere diameter = 400 nm) down to a single nanoparticle (with an in-plane width of about 20 nm) using single nanoparticle techniques [45]. The nanoparticle approach can deliver the same information as the SPR sensor, thereby minimizing its pixel size to the sub-100-nm regime. Because of the lower refractive index sensitivity, the LSPR nanosensor requires no temperature control, whereas the SPR sensor (with a large refractive index sensitivity) does. The final and most dramatic difference between the LSPR and SPR sensors is cost. Commercialized SPR instruments can cost between US $150,000 and 300,000 (plus supplies), whereas the prototype and portable LSPR system costs less than US $5,000 (plus supplies).

There is, however, a unifying relationship between these two seemingly different sensors. Both sensors' overall response can be described by using the following equation [81]:

$$\Delta\lambda_{max} = m\Delta n(1 - e^{-2d/l_d}) \quad (2)$$

where $\Delta\lambda_{max}$ is the wavelength shift response, m is the refractive index sensitivity, Δn is the change in refractive index induced by an adsorbate, d is the effective adsorbate layer thickness, and l_d is the characteristic electromagnetic field decay length. It is important to note that for planar SPR sensors, this equation quantitatively predicts an adsorbate's affect on the sensor. When applied to the LSPR nanosensor, this exponential equation approximates the response for adsorbate layers, but does provide a fully quantitative explanation of its response [18, 19]. Similar to the SPR sensor, the LSPR nanosensor's sensitivity arises from the distance dependence of the average induced square of the electric fields that extend from the nanoparticles' surfaces. This work provides important first steps towards the unified view of LSPR and SPR spectroscopies.

Conclusions

This work demonstrates the importance of nanoscale phenomenon and their implication in sensing applications. We have highlighted representative research accomplishments in the area of LSPR sensing using arrays of and single silver nanoparticles on surfaces. Specific demonstrations of using the LSPR as a signal transduction mechanism for chemosensing and biosensing applications on arrays of nanoparticles and on single nanoparticles were shown. Finally, direct comparisons between LSPR and SPR sensors were made. Both the SPR and LSPR sensors operate on the principle that small changes in refractive index at or near a noble metal's surface can be used to detect analyte binding at very low concentrations. While the sensors gain their sensitivities via different pathways, their overall sensitivities are approximately equivalent.

Acknowledgements We acknowledge support of the Nanoscale Science and Engineering Initiative of the National Science Foundation under NSF Award Number EEC-0118025. Any opinions, findings and conclusions, or recommendations expressed in this material are those of the authors and do not necessarily reflect those of the National Science Foundation. A.J. Haes also wishes to acknowledge the American Chemical Society Division of Analytical Chemistry and Dupont for a graduate fellowship. We are grateful for useful discussion and technical support provided by Adam McFarland.

References

1. Freeman RG, Grabar KC, Allison KJ, Bright RM, Davis JA, Guthrie AP, Hommer MB, Jackson MA, Smith PC, Walter DG, Natan MJ (1995) Science 267:1629–1632
2. Kahl M, Voges E, Kostrewa S, Viets C, Hill W (1998) Sens Actuators B 51:285–291
3. Schatz GC, Van Duyne RP (eds) (2002) Electromagnetic mechanism of surface-enhanced spectroscopy. Wiley, New York, p 759–774
4. Haynes CL, Van Duyne RP (2003) J Phys Chem B 107:7426–7433
5. Haynes CL, McFarland AD, Zhao L, Van Duyne RP, Schatz GC, Gunnarsson L, Prikulis J, Kasemo B, Käll M (2003) J Phys Chem B 107:7337–7342
6. Dirix Y, Bastiaansen C, Caseri W, Smith P (1999) Adv Mater 11:223–227
7. Haynes CL, Van Duyne RP (2003) Nano Lett 3:939–943
8. Maier SA, Brongersma ML, Kik PG, Meltzer S, Requicha AAG, Atwater HA (2001) Adv Mater 13:1501–1505
9. Maier SA, Kik PG, Atwater HA, Meltzer S, Harel E, Koel BE, Requicha AAG (2003) Nat Mater 2:229–232
10. Shelby RA, Smith DR, Schultz S (2001) Science (Washington, DC, US) 292:77–78
11. Andersen PC, Rowlen KL (2002) Appl Spectrosc 56:124A–135A
12. Haes AJ, Van Duyne RP (2002) J Am Chem Soc 124:10596–10604
13. Mucic RC, Storhoff JJ, Mirkin CA, Letsinger RL (1998) J Am Chem Soc 120:12674–12675
14. Hirsch LR, Jackson JB, Lee A, Halas NJ, West JL (2003) Anal Chem 75:2377–2381
15. Haes AJ, Van Duyne RP (2002) Mat Res Soc Symp Proc 723:O3.1.1–O3.1.6

16. Haes AJ, Van Duyne RP (2003) Laser Focus World 39:153–156
17. Haes AJ, Van Duyne RP (2003) SPIE 5221:47–58
18. Haes AJ, Zou S, Schatz GC, Van Duyne RP (2004) J Phys Chem B 108:6961–6968
19. Haes AJ, Zou S, Schatz GC, Van Duyne RP (2004) J Phys Chem B 108:109–116
20. Riboh JC, Haes AJ, McFarland AD, Yonzon CR, Van Duyne RP (2003) J Phys Chem B 107:1772–1780
21. Fritzsche W, Taton TA (2003) Nanotech 14:R63–R73
22. Aizpurua J, Hanarp P, Sutherland DS, Kall M, Bryant GW, Garcia de Abajo FJ (2003) Phys Rev Lett 90:057401/057401–057401/057404
23. Obare SO, Hollowell RE, Murphy CJ (2002) Langmuir 18:10407–10410
24. Nath N, Chilkoti A (2002) Proc SPIE-Int Soc for Opt Eng 4626:441–448
25. Nam J-M, Thaxton CS, Mirkin CA (2003) Science (Washington, DC, US) 301:1884–1886
26. Bailey RC, Nam J-M, Mirkin CA, Hupp JT (2003) J Am Chem Soc 125:13541–13547
27. Haynes CL, Van Duyne RP (2001) J Phys Chem B 105:5599–5611
28. Mulvaney P (2001) MRS Bulletin 26:1009–1014
29. El-Sayed MA (2001) Acc Chem Res 34:257–264
30. Link S, El-Sayed MA (1999) J Phys Chem B 103:8410–8426
31. Kreibig U, Gartz M, Hilger A, Hovel H (eds) (1998) Optical investigations of surfaces and interfaces of metal clusters. JAI Press, Stamford, pp 345–393
32. Mulvaney P (1996) Langmuir 12:788–800
33. Kreibig U (ed) (1997) Optics of nanosized metals. CRC Press, Boca Raton, pp 145–190
34. Hulteen JC, Treichel DA, Smith MT, Duval ML, Jensen TR, Van Duyne RP (1999) J Phys Chem B 103:3854–3863
35. Jensen TR, Malinsky MD, Haynes CL, Van Duyne RP (2000) J Phys Chem B 104:10549–10556
36. Michaels AM, Nirmal M, Brus LE (1999) J Am Chem Soc 121:9932–9939
37. Schultz S, Smith DR, Mock JJ, Schultz DA (2000) PNAS 97:996–1001
38. Yguerabide J, Yguerabide EE (1998) Anal Biochem 262:157–176
39. Kreibig U, Vollmer M (eds) (1995) Cluster materials. Springer Berlin Heidelberg New York, p 532
40. Taton TA, Lu G, Mirkin CA (2001) J Am Chem Soc 123:5164–5165
41. Taton TA, Mirkin CA, Letsinger RL (2000) Science 289:1757–1760
42. Sonnichsen C, Geier S, Hecker NE, von Plessen G, Feldmann J, Ditlbacher H, Lamprecht B, Krenn JR, Aussenegg FR, Chan VZ-H, Spatz JP, Moller M (2000) Appl Phys Lett 77:2949–2951
43. Sonnichsen C, Franzl T, Wilk T, von Plessen G, Feldmann J, Wilson O, Mulvaney P (2002) Phys Rev Lett 88:0774021–0774024
44. Bao P, Frutos AG, Greef C, Lahiri J, Muller U, Peterson TC, Wardern L, Xie X (2002) Anal Chem 74:1792–1797
45. McFarland AD, Van Duyne RP (2003) Nano Lett 3:1057–1062
46. Van Duyne RP, Haes AJ, McFarland AD (2003) SPIE 5223:197–207
47. Connolly S, Cobbe S Fitzmaurice D (2001) J Phys Chem B 105:2222–2226
48. Storhoff JJ, Lazarides AA, Mucic RC, Mirkin CA, Letsinger RL, Schatz GC (2000) J Am Chem Soc 122:4640–4650
49. Connolly S, Rao SN, Fitzmaurice D (2000) J Phys Chem B 104:4765–4776
50. Storhoff JJ, Elghanian R , Mucic RC, Mirkin CA, Letsinger RL (1998) J Am Chem Soc 120:1959–1964
51. Elghanian R, Storhoff JJ, RC Mucic, Letsinger RL, Mirkin CA (1997) Science 227:1078–1080
52. Mirkin CA, Letsinger RL, Mucic RC, Storhoff JJ (1996) Nature 382:607–609
53. Malinsky MD, Kelly KL, Schatz GC, Van Duyne RP (2001) J Am Chem Soc 123:1471–1482
54. Hilger A, Cuppers N, Tenfelde M, Kreibig U (2000) Eur Phys J D 10:115–118
55. Henglein A, Meisel D (1998) J Phys Chem B 102:8364–8366
56. Linnert T, Mulvaney P, Henglein A (1993) J Phys Chem 97:679–682
57. Kreibig U, Gartz M, Hilger A (1997) Ber Bunsen-Ges 101:1593–1604
58. Nath N, Chilkoti A (2002) Anal Chem 74:504-509
59. Eck D, Helm CA, Wagner NJ, Vaynberg KA (2001) Langmuir 17:957–960
60. Okamoto T, Yamaguchi I, Kobayashi T (2000) Opt Lett 25:372–374
61. Himmelhaus M, Takei H (2000) Sens Actuators B B63:24–30
62. Takei H (1998) Proc SPIE-Int Soc Opt Eng 3515:278–283
63. Lee PC, Meisel D (1982) J Phys Chem 86:3391–3395
64. Grabar KC, Freeman RG, Hommer MB, Natan MJ (1995) Anal Chem 67:735–743
65. Sun Y, Xia Y (2003) Proc SPIE Int Soc Opt Eng 5221:164–173
66. Sun Y, Mayers B, Herricks T, Xia Y (2003) Nano Lett 3:955–960
67. Sun Y, Xia Y (2003) Analyst (Cambridge, UK) 128:686–691
68. Sun Y, Xia Y (2003) Adv Mater (Weinheim, Germany) 15:695–699
69. Sun Y, Mayers B, Xia Y (2003) Nano Lett 3:675–679
70. Jin R, Cao YC, Hao E, Metraux GS, Schatz GC, Mirkin CA (2003) Nature (London, UK) 425:487–490
71. Storhoff JJ , Elghanian R, Mirkin CA, Letsinger RL (2002) Langmuir 18:6666–6670
72. Hulteen JC, Van Duyne RP (1995) J Vac Sci Technol A 13:1553–1558
73. Klar T, Perner M, Grosse S, von Plessen G, Spirkl W, Feldmann J (1998) Phys Rev Lett 80:4249–4252
74. Matsuo Y, Sasaki K (2001) Jpn J Appl Phys 40:6143–6147
75. Mock JJ , Oldenburg SJ, Smith DR, Schultz DA, Schultz S (2002) Nano Lett 2:465–469
76. Mock JJ, Smith DR, Schultz S (2003) Nano Lett 3:485–491
77. Green NM (1975) Adv Protein Chem 29:85–133
78. Jung LS, Campbell CT (2000) J Phys Chem B 104:11168–11178
79. Perez-Luna VH, O'Brien MJ, Opperman KA, Hampton PD, Lopez GP, Klumb LA, Stayton PS (1999) J Am Chem Soc 121:6469–6478
80. Liedberg B, Nylander C, Lundstroem I (1983) Sens Actuators 4:299–304
81. Jung LS, Campbell CT, Chinowsky TM, Mar MN, Yee SS (1998) Langmuir 14:5636–5648
82. Jung LS, Campbell CT (2000) Phys Rev Lett 84:5164–5167
83. Jung LS, Nelson KE, Stayton PS, Campbell CT (2000) Langmuir 16:9421–9432
84. Mann DA, Kanai M, Maly DJ, Kiessling LL (1998) J Am Chem Soc 120:10575–10582
85. Hendrix M, Priestley ES, Joyce GF, Wong C-H (1997) J Am Chem Soc 119:3641–3648
86. Frey BL, Jordan CE, Kornguth S, Corn RM (1995) Anal Chem 67:4482–4457
87. Mrksick M, Grunwell JR, Whitesides GM (1995) J Am Chem Soc 117:12009–12010
88. Rao J, Yan L, Xu B, Whitesides GM (1999) J Am Chem Soc 121:2629–2630
89. Berger CEH, Beumer TAM, Kooyman RPH, Greve J (1998) Anal Chem 70:703–706
90. Heaton RJ, Peterson AW, Georgiadis RM (2001) Proc Natl Acad Sci USA 98:3701–3704
91. Georgiadis R, Peterlinz KP, Peterson AW (2000) J Am Chem Soc 122:7837–3173
92. Jordan CE, Frutos AG, Thiel AJ, Corn RM (1997) Anal Chem 69:4939–4947

93. Nelson BP, Grimsrud TE, Liles MR, Goodman RM (2001) Anal Chem 73:1–7
94. Brockman JM, Frutos AG, Corn RM (1999) J Am Chem Soc 121:8044–8051
95. Brockman JM, Nelson BP, Corn RM (2000) Annu Rev Phys Chem 51:41–63
96. Hall D (2001) Anal Biochem 288:109–125
97. Schuck P (1997) Annu Rev Biophys Biomol Struct 26:541–566
98. Knoll W (1998) Annu Rev Phys Chem 49:569–638
99. Haake H-M, Schutz A, Gauglitz G (2000) Fresenius J Anal Chem 366:576–585
100. Shumaker-Parry JS, Zareie MH, Aebersold R, Campbell CT (2004) Anal Chem 76:918–929
101. Garland PB (1996) Q Rev Biophys 29:91–117
102. Shumaker-Parry JS, Campbell CT (2004) Anal Chem 76:907–917
103. Karlsson R, Stahlberg R (1995) Anal Biochem 228:274–280
104. Sjolander S, Urbaniczky C (1991) Anal Chem 63:2338–2345